Accepted Manuscript

One-step hydrothermal synthesis of a CoS_2@MoS_2 nanocomposite for high-performance supercapacitors

Feng Huang, Rongde Meng, Yanwei Sui, Fuxiang Wei, Jiqiu Qi, Qingkun Meng, Yezeng He

PII: S0925-8388(18)30338-4

DOI: 10.1016/j.jallcom.2018.01.324

Reference: JALCOM 44788

To appear in: *Journal of Alloys and Compounds*

Received Date: 17 January 2017

Revised Date: 23 January 2018

Accepted Date: 25 January 2018

Please cite this article as: F. Huang, R. Meng, Y. Sui, F. Wei, J. Qi, Q. Meng, Y. He, One-step hydrothermal synthesis of a CoS_2@MoS_2 nanocomposite for high-performance supercapacitors, *Journal of Alloys and Compounds* (2018), doi: 10.1016/j.jallcom.2018.01.324.

One-step hydrothermal synthesis of a CoS_2@MoS_2 nanocomposite for high-performance supercapacitors

Feng Huang [a], Rongde Meng [b], Yanwei Sui [a], Fuxiang Wei [a], Jiqiu Qi [a], Qingkun Meng [a], Yezeng He [a,*]

[a] *School of Materials Science and Engineering, China University of Mining and Technology, Xuzhou 221116, People's Republic of China*

[b] *Beijing Experimental School, Haidian, Beijing 100037, People's Republic of China*

Abstract

A MoS_2-coated CoS_2 composite has been prepared successfully via a one-step hydrothermal method. This CoS_2@MoS_2 hybrid material has a distinct morphology with few-layer MoS_2 wrapping the CoS_2 nanoparticles. Serving as a supercapacitor electrode, the obtained CoS_2@MoS_2 hybrid material exhibits a remarkable specific capacitance of 1038 F/g, a high rate capability of 71.7%, and excellent cycling stability of 84.76% retention after 10000 cycles. The superior electrochemical properties of the CoS_2@MoS_2 nanocomposite are attributed to the synergistic effects between the layered MoS_2 and conductive CoS_2.

Key words: MoS_2; CoS_2; flower-like structure; supercapacitors

1. Introduction

Supercapacitors have attracted worldwide attention due to their excellent properties, such as rapid recharge ability, high power density, long cycle life, eco-friendly nature and low-cost preparation [1-3]. There are two major types of supercapacitors that are related to the different charge storage mechanisms. The first type is a double-layer capacitor, which accumulates charge at the electrode-electrolyte interface by establishing a Helmholtz double-layer [4-7], and the second type is a pseudo-capacitor based on a redox capacitive mechanism [8-11].

Graphene, a two-dimensional carbon allotrope, has attracted considerable attention due to its fascinating properties and broad applications in nanoelectronic devices since its discovery in 2004 [12]. However, graphene materials also have several disadvantages such as high costs, low yield and poor scalability [13,14]. MoS_2

*Corresponding author, E-mail: hyz0217@hotmail.com

is a transition metal sulfide with a layered structure. The ultrathin thickness and 2D morphology enable MoS_2 to achieve ultrahigh specific surface areas compared to its bulk counterpart [15,16]. Mo atoms can easily prompt redox faradaic reactions in the interlayer space due to oxidation states spanning a range from +2 to +6, and its theoretical specific capacitance could be as high as 1000 F/g [17,18]. Therefore, the layered structure and redox faradaic reactions play important roles in making the MoS_2 a promising electrode material used in the supercapacitors. To date, many studies regarding the use of MoS_2 in supercapacitors have been reported. For example, Ramadoss et al. prepared a mesoporous MoS_2 nanostructure by a hydrothermal method and obtained maximum capacitance values of 376 and 403 F/g at a scan rate of 1 mV/s in 1 M Na_2SO_4 and KCl electrolyte solutions, respectively [19]. Wang et al. synthesized hierarchical MoS_2 nanospheres for supercapacitors by a hydrothermal method and demonstrated a capacitance of 142 F/g at a current density of 0.59 A/g [20]. Zhou et al. reported flower-like MoS_2 nanospheres that were synthesized by a hydrothermal route and showed specific capacitances of 122 F/g at 1 A/g or 114 F/g at 2 mV/s [21]. Krishnamoorthy et al. synthesized few-layered MoS_2 nanosheets by using a mechanical milling method and demonstrated a MoS_2 based wire type solid state supercapacitors device with a specific capacitance of 119 $\mu F/cm^{-1}$ [22]. Nevertheless, the preparation of a high-performance supercapacitors using MoS_2 as an electrode material is still a challenging task due to the low electrical conductivity and low number of accessible active sites in MoS_2.

To overcome these difficulties, MoS_2 should be combined with a conductive material with high electrochemical activity to enhance the electrical conductivity and increase content of accessible active sites [23,24]. As an important transition metal sulfide, CoS_2 has the best conductivity and thermal stability among the entire cobalt sulfide family, such as CoS, Co_3S_4, Co_4S_3, Co_2S_3 and Co_9S_8 [25,26]. CoS_2 has a superior capacitive behavior because its negative Gibbs free energy value causes a spontaneous thermodynamic reduction reaction that is useful for pseudo-capacitance supercapacitors [27,28]. Xing et al. have successfully prepared a type of octahedral-shaped CoS_2 with a specific capacitance of 236.5 F/g at 1 A/g in 2 M KOH

[29]. Ren et al. synthesized CoS_2 nanowires deposited on a graphite disc using a hydrothermal method with a specific capacitance of 828.2 F/g at 10 mV/s in 6 M KOH [30].

In this work, we synthesized a novel CoS_2@MoS_2 nanocomposite by a facile one-step hydrothermal technique. The CoS_2@MoS_2 nanocomposite electrode shows a high specific performance of 1038 F/g at 1 A/g in 2 M KOH solution. In addition, the CoS_2@MoS_2 nanocomposite electrode showed excellent cyclic stability and a high rate capability contrasted with pure MoS_2 and pure CoS_2. The capacitance remained approximately 84.76% after 10000 cycles of charge-discharge at a current density of 5 A/g. The synergistic effect between MoS_2 and CoS_2 in the composite is expected to improve electrode performance when used as an electrode material for supercapacitors.

2. Experimental section

2.1 Materials

All the reagents used in this experiment were of analytical grade and were used without purification. Thiocarbamide (NH_2CSNH_2), sodium molybdatedihydrate ($Na_2MoO_4{\cdot}2H_2O$), cobalt (II) nitrate hexahydrate ($Co(NO_3)_2{\cdot}6H_2O$) and anhydrous ethanol (C_2H_6O) were purchased from Aladdin Industrial Corporation (ShangHai). The water was purified through a Lab Pure Water System (18.25 mΩ).

2.2 Synthesis of MoS_2, CoS_2 and CoS_2@MoS_2 nanocomposites

The CoS_2@MoS_2 nanocomposite was synthesized through a facile solvothermal method. Initially, 2.5 mmol $Na_2MoO_4{\cdot}2H_2O$, 1.25 mmol $Co(NO_3)_2{\cdot}6H_2O$ (at a Mo:Co molar ratio of 2:1) and 6.25 mmol H_2NCSNH_2 were dissolved in a 30 ml mixed solution of DI water and anhydrous ethanol (1:1 in volume). The precursor solution was magnetically stirred by ultrasonication for 30 min. The mixture was then transferred into a Teflon-lined autoclave, sealed, and heated in an oven at 180 °C for 48 hours. After natural cooling to room temperature, the resulting black solid product was collected, then washed with DI water three times and ethanol three times before drying in vacuum at 70 °C (referred to as CM-2). The number “2” refers to the molar ratio of $Na_2MoO_4{\cdot}2H_2O$ and $Co(NO_3)_2{\cdot}6H_2O$. CM-1 and CM-3 were synthesized by

the addition of the corresponding quantity of $Co(NO_3)_2 \cdot 6H_2O$ into the mixture with the same amount of $Na_2MoO_4 \cdot 2H_2O$ (2.5 mmol). As reference materials, pristine MoS_2 and CoS_2 were also prepared, following the same procedure in the absence of $Co(NO_3)_2 \cdot 6H_2O$ and $Na_2MoO_4 \cdot 2H_2O$, respectively.

2.3 Characterization

The CoS_2@MoS_2 (CM-2) samples were characterized for structural properties using X-ray diffraction (D8 Advance, Bruker, Germany) with Cu-Kα radiation in the angle range from 5°-85° at a scan rate of 8 °/min. The surface area and nitrogen absorption-desorption isotherm were analyzed using an ASAP 2020 analyzer. XPS spectra were recorded on ESCALAB 250Xi using Al-Kα radiation as the X-ray source. The morphology and structure of the products were characterized using field emission SEM (Hitachi SU-8000) equipped with high-resolution TEM (HRTEM, Tecnai G2F20).

2.4 Electrochemical measurements

Electrochemical measurements were performed on a CHI660D (Chenhua, Shanghai, China) electrochemical workstation in a 2 M KOH aqueous electrolyte solution using a three-electrode system that consists of a working electrode, a platinum plate counter electrode, and a saturated calomel electrode (SCE, reference electrode) at room temperature. The working electrode was prepared by mixing the as-prepared active material, acetylene black and polyvinylidene fluoride (PVDF) in N-methylpyrrolidinone (NMP) according to a ratio of 80:10:10. The resultant slurry was pasted on nickel foam (1×2 cm^2) serving as a current collector, which was then dried at 80 °C for 12 h and pressed on 10 MPa. The mass of the activated material was obtained by a weight difference method using a sensitive microbalance. Finally, the loading masses of MoS_2, CoS_2 and CoS_2@MoS_2 on the Ni foam were 1.1, 0.78 and 0.9 mg/cm^2, respectively. Cyclic voltammetry measurements were carried out in a potential range from 0 to 0.65 V (vs. SCE) at different scan rates in a 2 M KOH electrolyte. Galvanostatic charge-discharge measurements were performed at different current densities (1, 2, 5, and 10 $A \cdot g^{-1}$) for the as-prepared electrodes. The specific capacitance can be calculated from the galvanostatic charge-discharge curve

according to Eq. (1)

$$C = \frac{I\Delta t}{m\Delta v} \quad (1),$$

where C is the specific capacitance, I is the current, Δt is the discharge time, Δv is the potential window, and m is mass of the electroactive material. Electrochemical impedance spectroscopy (EIS) measurements were conducted by applying an AC voltage with 5 mV amplitude in the frequency range from 0.01 Hz to 100 KHz.

3. Results and discussion

The CoS_2@MoS_2 (CM-1, 2, 3) nanostructures were prepared using a low-temperature hydrothermal method. During the reaction, the active species (S^{2-} ions) are released from NH_2CSNH_2 according to Eq. (2). The S^{2-} ions react with dilute nitric acid to produce elemental sulfur (Eq. (3)). In addition, the elemental sulfur plays an important role in the chemical reactions (Eq. (4)). Lastly, the S^{2-} ions interacted with MoO_4^{2-} ions to produce MoS_2 (Eq. (5)).

$$H_2NCSNH_2 + H_2O \rightarrow 2NH_3 + 2H_2S + CO_2 \qquad (2)$$

$$6H_2S + 4HNO_3 \rightarrow 6S + 4NO + 5H_2O \qquad (3)$$

$$H_2S + S + Co^{2+} \rightarrow CoS_2 + 2H^+ \qquad (4)$$

$$MoO_4^{2-} + H_2S \rightarrow MoS_2 + 3H_2 + SO_4^{2-} \qquad (5)$$

The crystal structure and phase purity of the as-prepared samples were characterized by XRD. Fig. 1a shows the XRD pattern of the as-prepared flowerlike CoS_2@MoS_2 nanostructured sample. The curve shows several sharp peaks at 14.3°, 29.2°, 32.6°, 39.5°, 49.7°, 52.08°, 58.43°, 60.1°, 68.4°, 72.7° and 75.9° which can be assigned to the (002), (004), (100), (103), (105), (018), (110), (008), (200), (203) and (116) planes of hexagonal MoS_2 (JCPDS 37-1942), respectively. The peaks at 32.3°, 36.23°, 39.8°, 46.3°, 60.2° and 69.8° correspond to the (200), (210), (211), (220), (230) and (410) planes of CoS_2 (JCPDS 65-3322), respectively [31,32]. Table 1 lists the textural properties (pore volume, BET surface area and pore size) of MoS_2, CoS_2@MoS_2 and CoS_2. Clearly, CoS_2@MoS_2 exhibits the largest pore volume, BET surface and pore size. Due to the presence of flowerlike MoS_2, the BET surface of CoS_2@MoS_2 increases to 60.1 m^2/g compared with a value of 51.2 for pure CoS_2.

Moreover, the pores were mainly distributed in the range of 2-20 nm. Such a high-surface-area microstructure contains many active sites for electrochemical interactions with electrolyte ions, which is very useful for energy storage applications.

Table 1 Textural properties of MoS_2, CoS_2@MoS_2 and CoS_2.

Materials	Pore volume (cm^3/g)	BET surface area (m^2/g)	Pore size (nm)
MoS_2	0.129	58.2	8.9
CoS_2@MoS_2 (CM-2)	0.165	60.1	10.9
CoS_2	0.112	51.2	7.6

XPS was carried out to obtain information regarding the structure and the electronic state of Mo, Co and S of the as-prepared nanocomposite. As shown in Fig. 2a, the survey scan of the CoS_2@MoS_2 nanostructured electrode exhibits characteristic peaks of the Mo 3d, Co 2p, S 2p, O 1s and C 1s levels at their corresponding binding energies. Fig. 2b shows that the high-resolution scans of the Mo 3d electrons exhibit two primary peaks at 228.9 and 232.2 eV that correspond to the Mo $3d_{3/2}$ and $3d_{5/2}$ in MoS_2, respectively, which further confirms the formation of MoS_2. The peak at 232.8 eV is attributed to the existence of a small amount of Mo^{6+} due to MoS_2 exposure to the air. The emergence of a peak at 226.0 eV corresponds to the S 2s orbitals of MoS_2. Fig. 2c shows two dominating peaks at 779.8 eV and 794.7 eV that correspond to Co $2p_{3/2}$ and $2p_{1/2}$, respectively. The two peaks at 161.4 eV and 162.8 eV correspond to the S $2p_{3/2}$ and $2p_{1/2}$ levels of divalent sulfide ions (S^{2-}). The peak at 163.4 eV indicates the presence of bridging S_2^{2-} or apical S^{2-} [33,34].

The morphologies of the CoS_2@MoS_2 nanocomposites (the samples are referred to as CM-1, CM-2 and CM-3) were examined by FESEM. As shown in Fig. 3, CM-2 presents a flowerlike morphology and is quite different from CM-1 and CM-3. In addition, inductively coupled plasma (ICP) analysis was conducted to determine the molar percentage between CoS_2 and MoS_2 in CM-1, CM-2 and CM-3, as shown in

Table 2.

Table 2. The molar content of MoS_2 and CoS_2 in CM-1, CM-2 and CM-3.

Samples / Component	CM-1	CM-2	CM-3
MoS_2	42.9%	74.9%	87.5%
CoS_2	57.1%	25.1%	12.5%

Fig. 4 shows the morphologies of MoS_2, CoS_2 and CoS_2@MoS_2 (CM-2) nanocomposites. The images indicate that the CoS_2@MoS_2 nanocomposite has a similar morphology to MoS_2. MoS_2 (Fig. 4a,b) and CM-2 (Fig. 4e,f) are both flowerlike, whereas CoS_2 is sphere-like. The size of the CM-2 nanocomposite is much smaller than that of either MoS_2 or CoS_2. Hence, the CM-2 nanocomposite has a large surface area that provides plenty of active sites for an electrochemical reaction.

Fig. 5 shows the TEM images of the synthesized CM-2 composite. It can be seen that the MoS_2 sheets exhibit only a few layers located at the edge of CM-2 (Fig. 5a,b). The interconnected nanosheets of MoS_2 still maintain a flowerlike morphology, and several CoS_2 nanoparticles embedded among the flowerlike MoS_2 nanosheets are recognized in Fig. 5a (black area). The CoS_2 nanoparticles serve as substrates for the growth of MoS_2 nanoplates and are highly likely to increase the conductivity of the composites. The high-resolution TEM (HRTEM) images of CM-2 in Fig. 5 (c,d inset) demonstrate that the interlayer spacing of MoS_2 in the composite is 0.62 nm, and interplanar spacing of the CoS_2 sheets is 0.24 nm, which are both consistent with previous reports [35,36].

To explore the potential applications of the CoS_2@MoS_2 nanocomposite for supercapacitors, we have tested the electrochemical properties of the CM-1, CM-2 and CM-3 nanocomposite electrodes by cyclic voltammetry (CV) and galvanostatic charge/discharge (GCD) measurements, as shown in Fig. 6a,b. The CV curves of CM-1, CM-2 and CM-3 were obtained at a scan rate of 5 mV/s in the potential window of 0.0-0.65 V versus SCE in 2 M KOH. Fig. 6b illustrates the charge–discharge curves of CM-1, CM-2 and CM-3 in the potential range of 0–0.5 V

at a current density of 1 A/g. The CM-2 nanocomposite shows the best charge storage properties. The specific capacitance can be calculated by Eq. (1), and the specific capacitance of the prepared CM-2 was calculated to be 1038 F/g, which is greater than that of both CM-1 (508 F/g) and CM-3 (468 F/g). Next, CM-2 was taken as an example for comparison with pure MoS_2 and pure CoS_2. As shown in Fig. 6c, the significant increase in the integrated area indicates that the composite has a higher capacity. For the curves of the CM-2 composite, the characteristic oxidation and reduction positions (oxidation peak around +0.52 V and reduction peak around +0.24 V) are related to faradaic redox reactions between the Co^{2+} and Co^{3+} states of cobalt in an alkaline KOH electrolyte [37,38]. The main reaction mechanism can be described as follows,

$$CoS_2 + OH- \leftrightarrow CoS_2OH + H_2O + e^- \quad (6)$$

$$\mathrm{MoS_2} + K^+ + e^- \leftrightarrow MoS - SK^+ \quad (7)$$

The supercapacitive characteristics can also be measured by a constant current charge-discharge cycling test. Fig. 6d shows the GCD curves for MoS_2, CoS_2 and CM-2 at a current density of 1 A/g. The specific capacitance values were calculated to be 116.8 and 464.4 F/g for the MoS_2 and CoS_2, respectively, while the specific capacitance of CM-2 composite attained 1038 F/g. Fig. 6e shows the specific capacitances of the MoS_2, CoS_2 and CM-2 electrodes as a function of the current density. The specific capacitance retention of CM-2 is higher than that of MoS_2 and CoS_2, which can be up to 71.7% when the current density changes from 1 A/g to 10 A/g. Typical impedance plots for this electrode are displayed in Fig. 7f. The equivalent series resistance (Rs) of the MoS_2, CoS_2@MoS_2 and CoS_2 electrodes are measured to be 0.56171, 0.34692 and 0.59254 Ω, respectively (Fig. 6f inset). The charge transfer resistance (Rct) of the MoS_2, CM-2 and CoS_2 electrodes are 0.8686, 0.1303 and 0.46718 Ω, respectively. These results indicate that the conductivity of CM-2 has increased significantly due to the existence of CoS_2 [39,40]. The smaller Rs and Rct values indicate a lower resistance and better capacitive behavior.

Cycle measurements were performed to further evaluate the electrochemical performance of the MoS_2, CoS_2 and CM-2. The cycling stabilities of the MoS_2, CoS_2

and the CM-2 electrodes were tested by repeating the GCD measurements between 0.0 and 0.5 V (vs. SCE) at a current density of 5 A/g for 10000 cycles. As shown in Fig. 7, the capacitance retention values of MoS_2, CoS_2 and CM-2 in a 2 M KOH electrolyte are 57.02%, 80.71% and 84.76% after 10000 cycles, which indicates that CM-2 has the best cycling stability.

The excellent electrochemical properties of CM-2 are attributed to the synergistic effect of MoS_2 and CoS_2: (1) Layered MoS_2 forms ion-buffering reservoirs to improve the ion diffusion rate within the prepared materials; (2) the nanoscale size of the CM-2 composite increases the specific surface area and greatly shortens the diffusion route through which both ions and electrons transfer during the charge-discharge process; (3) the presence of MoS_2 as a CoS_2 substrate in the composite system not only maintains a flower-like structure but also provides a path for the insertion and extraction of ions within the composite to increase the reaction rate; and (4) the conductive CoS_2 nanoparticles could efficiently lower the internal resistance and provide perfect continuous channels for electron transportation. Hence, the electrochemical performance of CM-2 is better than that of pure MoS_2 or CoS_2 due to the presence of two components with complementary properties.

4. Conclusions

In summary, the CoS_2@MoS_2 nanocomposite has been synthesized via a facile one-step hydrothermal method. In contrast to pure MoS_2 and pure CoS_2, the specific capacitance and rate capability of the CoS_2@MoS_2 (CM-2) nanocomposite has been greatly enhanced. Furthermore, the CoS_2@MoS_2 (CM-2) nanocomposite displays an excellent long-time cycling stability, retaining 84.76% of the initial capacitance after 10000 cycles at a current density of 5 A/g. These excellent results indicate that the CoS_2@MoS_2 nanocomposite is a promising and suitable electrode material for high-performance supercapacitors.

Acknowledgments

The authors would like to acknowledge the support by the National Natural Science Foundation of China (Grant No. 51501221) and the China Postdoctoral Science Foundation (No. 2016M591954).

References

1. P. Simon, Y. Gogotsi, Materials for electrochemical capacitors, Nat Mater. 7 (2008) 845-854.

2. M.D. Stoller, S. Park, Y. Zhu, J. An, R.S. Ruoff, Graphene-based ultracapacitors, Nano Lett. 8 (2008) 3498-3502.

3. L.L. Zhang，X.S. Zhao, Carbon-based materials as supercapacitor electrodes, Chem Soc Rev. 38 (2009) 2520-2531.

4. Z. Yu， L. Tetard, L. Zhai, J. Thomas, Supercapacitor electrode materials: nanostructures from 0 to 3 dimensions. Enger Environ Sci. 8 (2015) 702-730.

5. C. Du, N. Pan, Carbon Nanotube-Based Supercapacitors. Nanotechnology Law & Business. 4 (2007) 625-634.

6. G.S. Gund, D.P. Dubal, S.S. Shinde, Architectured morphologies of chemically prepared NiO/MWCNTs nanohybrid thin films for high performance supercapacitors. Acs Appl Mater Inter. 6 (2014) 3176-3188.

7. Z. Niu, L. Zhang, L. Liu, All-solid-state flexible ultrathin micro-supercapacitors based on graphene. Adv Mater. 25 (2013) 4035-4042.

8. N. Chodankar, G. Gund, D. Dubal, Alcohol mediated growth of a-MnO_2 thin films from $KMnO_4$ precursor for high performance supercapacitors. Rsc Adv, 2014.

9. X. Lu, D. Zheng, T. Zhai, Large-area manganese oxide nanorod arrays as high-performance electrochemical supercapacitor. Enger Environ Sci. 4 (2011) 2915-2921.

10. J.H. Kim, K. Zhu, Y. Yan, Microstructure and pseudocapacitive properties of electrodes constructed of oriented NiO-TiO_2 nanotube arrays. Nano Lett. 10 (2010) 4099-4104.

11. G. Ma, H. Peng, J. Mu, In situ intercalative polymerization of pyrrole in graphene analogue of MoS_2, as advanced electrode material in supercapacitor. J Power Source. 229 (2013) 72-78.

12. K.S. Novoselov, A.K. Geim, S.V. Morozov, Electric Field Effect in Atomically Thin Carbon Films. Science. 306 (2004) 666-669.

13. A. Reina, X. Jia, J. Ho, Large Area, Few-Layer Graphene Films on Arbitrary

Substrates by Chemical Vapor Deposition. Nano Lett. 9 (2009) 655-663.

14. D.V. Kosynkin, A.L. Higginbotham, A. Sinitskii, Longitudinal unzipping of carbon nanotubes to form graphene nanoribbons. Nature. 458 (2009) 872-876.

15. X. Cao, C. Tan, X. Zhang, Solution-Processed Two-Dimensional Metal Dichalcogenide-Based Nanomaterials for Energy Storage and Conversion. Adv Mater. 28 (2016) 6167-6196.

16. G. Du, Z. Guo, S. Wang, Superior stability and high capacity of restacked molybdenum disulfide as anode material for lithium ion batteries. Chem Commun. 46 (2010) 1106-1108.

17. F. Huang, A.Yan, Y. Sui, F. Wei, J. Qi, Q. Meng,. One-step hydrothermal synthesis of Ni_3S_4@MoS_2 nanosheet on carbon fiber paper as a binder-free anode for supercapacitor. *J Mater Sci-Mater El, 28* (2017) 12747-12754.

18. L. Cao, S. Yang, W. Gao, Direct laser-patterned micro-supercapacitors from paintable MoS_2 films. Small. 9 (2013) 2905.

19. A. Ramadoss, T. Kim, G.S. Kim, Enhanced activity of a hydrothermally synthesized mesoporous MoS_2 nanostructure for high performance supercapacitor applications. New J Chem. 38 (2014) 2379-2385.

20. L. Wang, M. Ying, Y. Min,. Hierarchical hollow MoS_2 nanospheres with enhanced electrochemical properties used as an Electrode in Supercapacitor. Electrochim Acta. 186 (2015) 391-396.

21. X. Zhou, B. Xu, Z. Lin, Hydrothermal synthesis of flower-like MoS_2 nanospheres for electrochemical supercapacitors. J Nanosci Nanotechno. 14 (2014) 7250-7254.

22. K. Krishnamoorthy, P. Pazhamalai, G.K. Veerasubramani, Mechanically delaminated few layered MoS_2 nanosheets based high performance wire type solid-state symmetric supercapacitors. J Power Source. 321 (2016) 112-119.

23. C. Xu, S. Peng, C. Tan, Ultrathin S-doped $MoSe_2$ nanosheets for efficient hydrogen evolution. J. Mater. Chem A. 2 (2014) 5597-5601.

24. H. Tang, J. Wang, H. Yin, Growth of polypyrrole ultrathin films on MoS_2 monolayers as high-performance supercapacitor electrodes. Adv. Mater. 27 (2015) 1117-1123.

25. Q. Wang, L. Jiao, Y. Han, CoS_2 Hollow Spheres: Fabrication and Their Application in Lithium-Ion Batteries. J. Phys. Chem C. 115 (2011) 8300-8304.

26. H. Yamada, K. Terao, M. Aoki. Electronic structure and magnetic properties of CoS_2. J. Magn Magn Mater. 177 (1998) 607-608.

27. B. Wang, J. Park, D. Su, C. Wang, H. Ahn, Solvothermal synthesis of CoS_2-graphene nanocomposite material for high-performance supercapacitors. J. Mater. Chem. 22 (2012) 15750-15756.

28. S. Amaresh, K. Karthikeyan, I.C. Jang, Single-step microwave mediated synthesis of the CoS_2 anode material for high rate hybrid supercapacitors. J. Mater Chem. 2 (2014) 11099-11106.

29. J.C. Xing, Y.L. Zhu, Q.W. Zhou, Fabrication and shape evolution of CoS_2 octahedrons for application in supercapacitors. Electrochim Acta. 136 (2014) 550-556.

30. R. Ren, M.S. Faber, R. Dziedzic, Metallic CoS_2 nanowire electrodes for high cycling performance supercapacitors. Nanotechnology. 26 (2015) 494001.

31. K.S. Liang, R.R. Chianelli, F.Z. Chien, Structure of poorly crystalline MoS_2,-A modeling study. J. Non-Cryst Solids. 79 (1986) 251-273.

32. L. Zhang, H.B. Wu, X.W. Lou, Unusual CoS_2 ellipsoids with anisotropic tube-like cavities and their application in supercapacitors. Chem Commun. 48 (2012) 6912-6914.

33. Y.R. Liu, W.H. Hu, X. Li, Facile one-pot synthesis of CoS_2 -MoS_2 /CNTs as efficient electrocatalyst for hydrogen evolution reaction. Appl Surf Sci.384 (2016) 51-57.

34. A. Ramadoss, T. Kim, G.S. Kim, Enhanced activity of a hydrothermally synthesized mesoporous MoS_2 nanostructure for high performance supercapacitor applications. New J. Chem. 38 (2014) 2379-2385.

35. C. Hao, F. Wen, J. Xiang, Controlled Incorporation of $Ni(OH)_2$ Nanoplates Into Flowerlike MoS_2 Nanosheets for Flexible All-Solid-State Supercapacitors. Adv Funct Mater. 24 (2014) 6700–6707.

36. C. Su, J. Xiang, F. Wen, Microwave Synthesized Three-dimensional Hierarchical Nanostructure CoS_2/MoS_2 Growth on Carbon Fiber Cloth: A Bifunctional Electrode for Hydrogen Evolution Reaction and Supercapacitor. Electrochim Acta. 212 (2016) 941-949.

37. J.C Xing, Y. L. Zhu, M.Y. Li, Hierarchical mesoporous CoS_2 microspheres: Morphology-controlled synthesis and their superior pseudocapacitive properties. Electrochim Acta. 14 (2014) 9285–9292.

38. A.Ramadoss, T.Kim, G.S.Kim, J.K.Sang, Enhanced activity of a hydrothermally synthesized mesoporous MoS_2 nanostructure for high performance supercapacitor

applications. New. J. Chem. 38 (2014) 2379-2385.

39. K.J. Huang, L. Wang, Y.J. Liu, Layered MoS_2–graphene composites for supercapacitor applications with enhanced capacitive performance. Int J Hydrogen Enger. 38 (2013) 14027-14034.

40. L. Wang, M. Ying, Y. Min, Hierarchical hollow MoS_2 nanospheres with enhanced electrochemical properties used as an Electrode in Supercapacitor. ElectrochimActa. 186 (2015) 391-396.

Figure Captions

Fig. 1 (a) XRD pattern of the CoS_2@MoS_2 (CM-2) nanocomposite. N_2 sorption isotherms of (b) MoS_2; (c) CoS_2@MoS_2 (CM-2); and (d) CoS_2. Inset: the pore size distribution curve.

Fig. 2 XPS spectra of the CoS_2@MoS_2 nanocomposite: (a) survey; (b) Mo 3d; (c) Co 2p; and (d) S 2p.

Fig. 3 SEM images of a,d) CM-1, b,e) CM-2, and c,f) CM-3.

Fig. 4 SEM images of (a,b) pure MoS_2; (c,d) pure CoS_2; and the (e,f) CoS_2@MoS_2 nanocomposite.

Fig. 5 TEM (a,b) and HRTEM(c,d) of the CoS_2@MoS_2 nanocomposite.

Fig. 6 (a) Cyclic voltammograms curves of CM-1, CM-2 and CM-3. (b) Galvanostatic charging/discharging curves of CM-1, CM-2 and CM-3. (c) Cyclic voltammograms of MoS_2, CoS_2 and CoS_2@MoS_2. (d) Galvanostatic charging/discharging curves of MoS_2, CoS_2 and CoS_2@MoS_2. (e) Rate capability curves of MoS_2, CoS_2 and CoS_2@MoS_2. (f) Nyquist plots of MoS_2, CoS_2 and CoS_2@MoS_2 electrode.

Fig. 7 Cycling performance plots of MoS_2, CoS_2 and CoS_2@MoS_2.

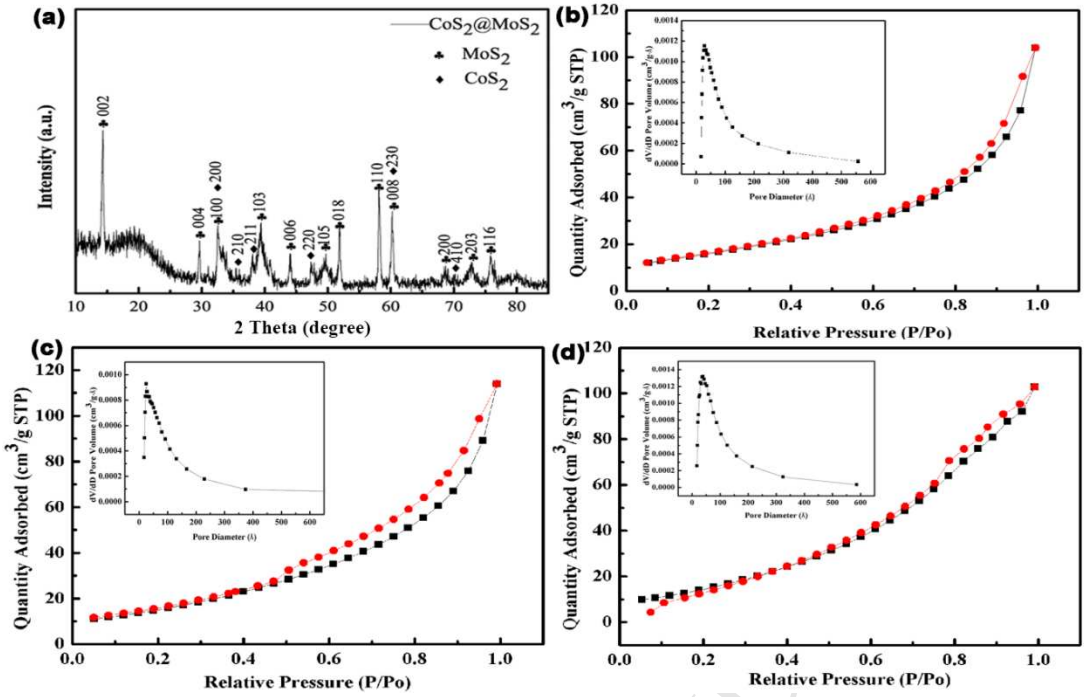

Figure 1

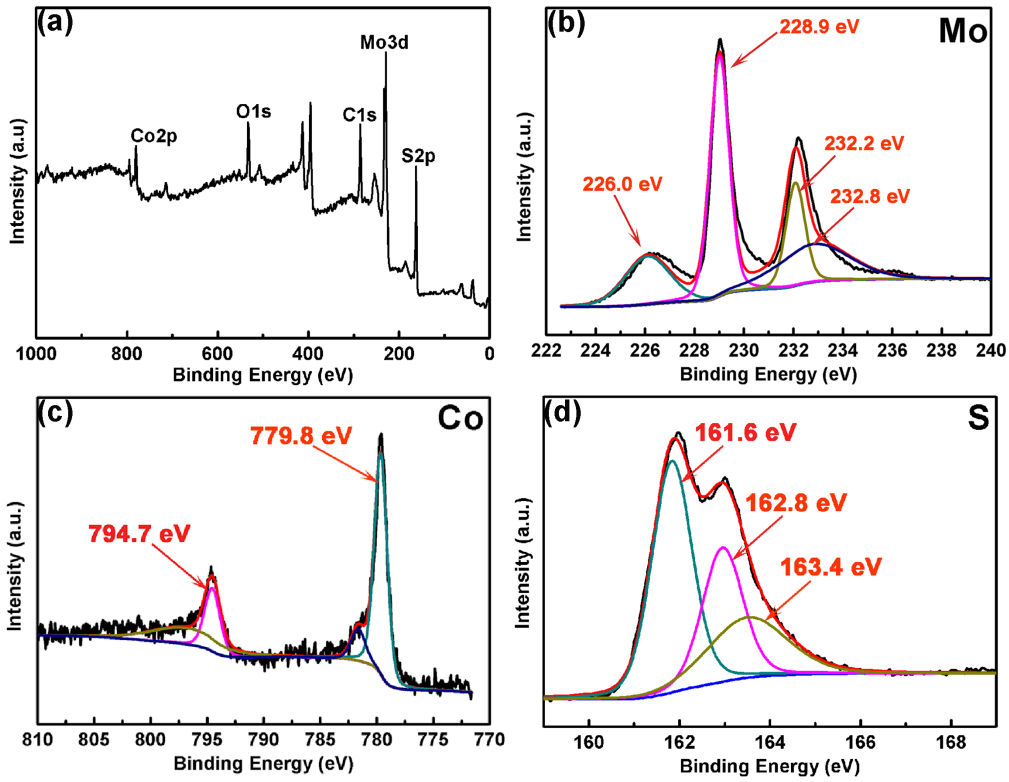

Figure 2

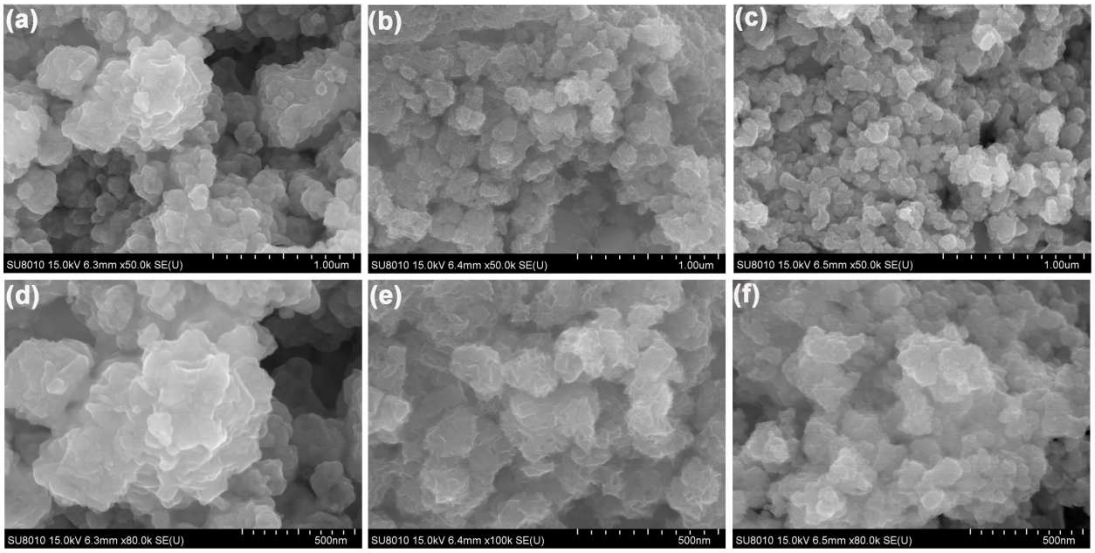
(a)
SU8010 15.0kV 6.3mm x50.0k SE(U)
1.00um
(b)
SU8010 15.0kV 6.4mm x50.0k SE(U)
1.00um
(c)
SU8010 15.0kV 6.5mm x50.0k SE(U)
1.00um
(d)
SU8010 15.0kV 6.3mm x80.0k SE(U)
500nm
(e)
SU8010 15.0kV 6.4mm x100k SE(U)
500nm
(f)
SU8010 15.0kV 6.5mm x80.0k SE(U)
500nm

Figure 3

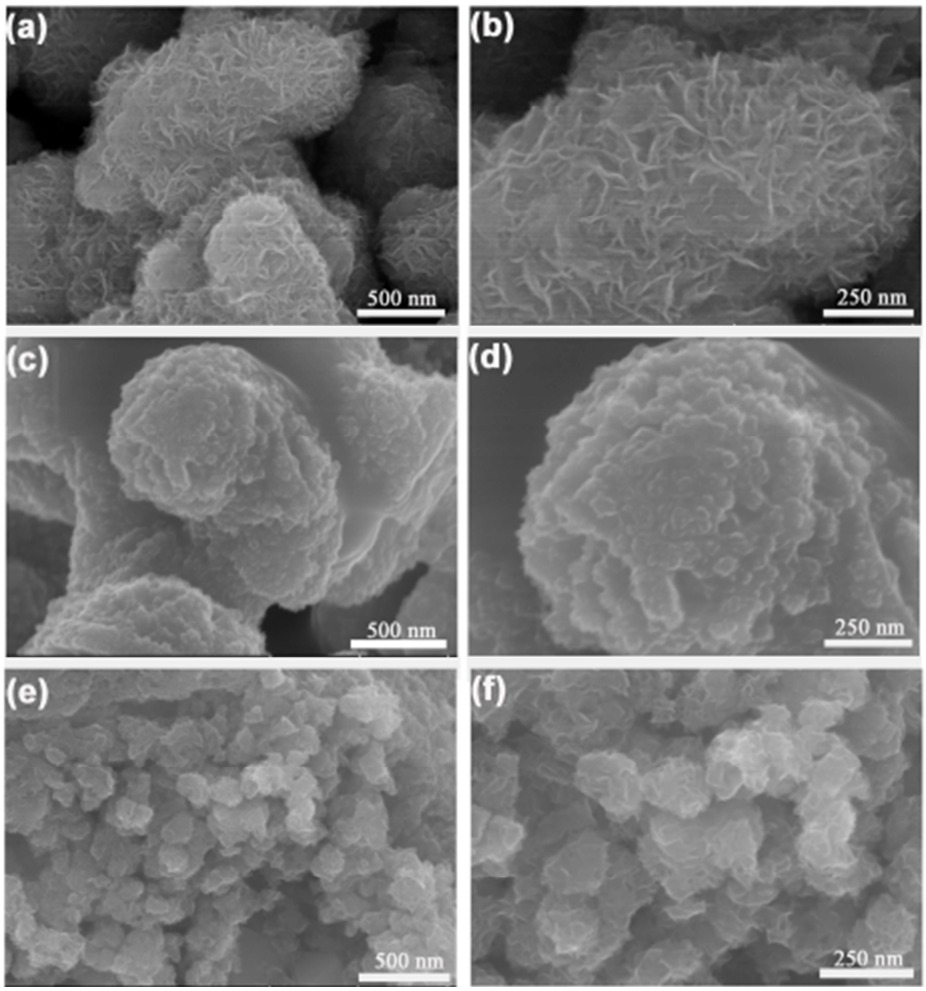
(a)
500 nm
(b)
250 nm
(c)
500 nm
(d)
250 nm
(e)
500 nm
(f)
250 nm

Figure 4

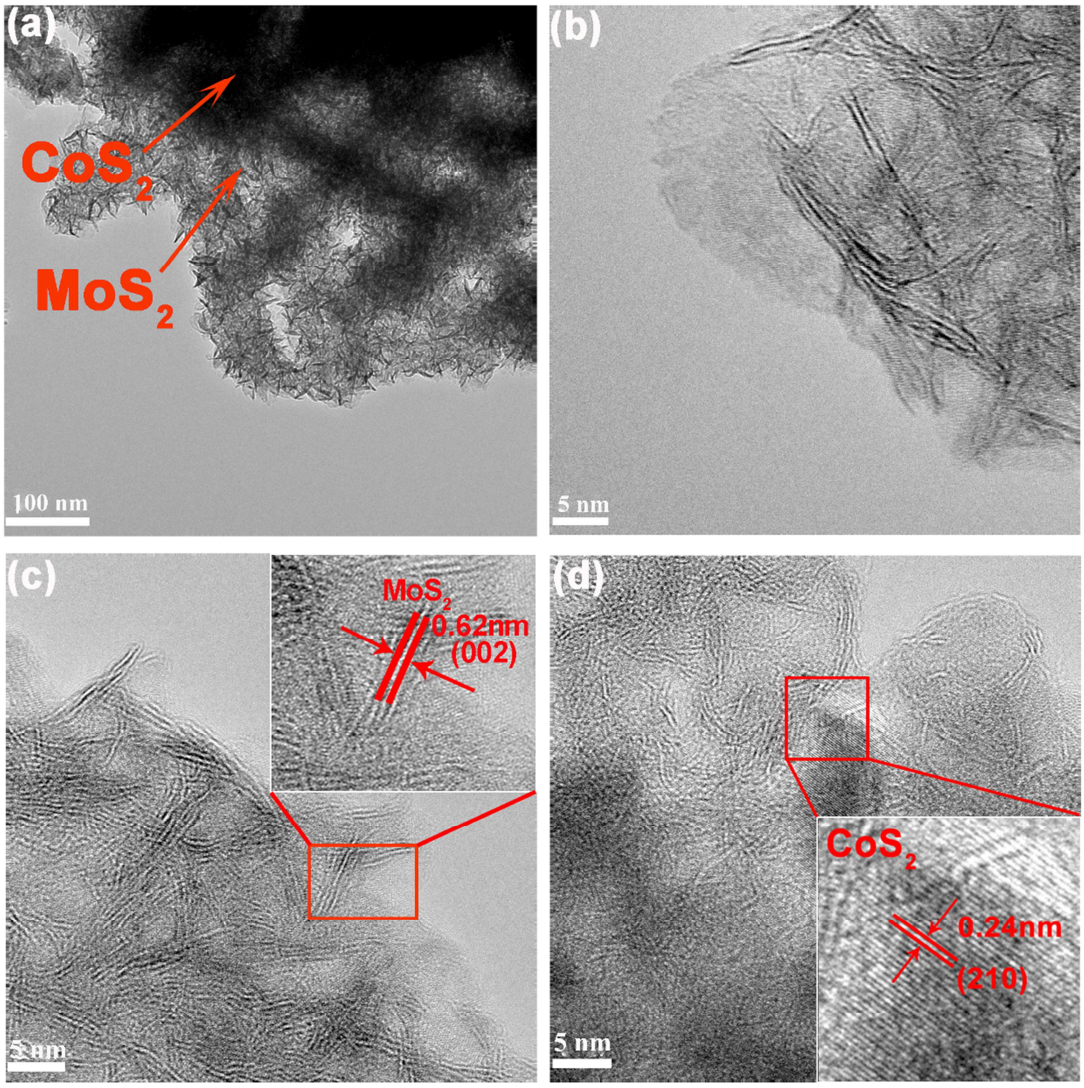

Figure 5

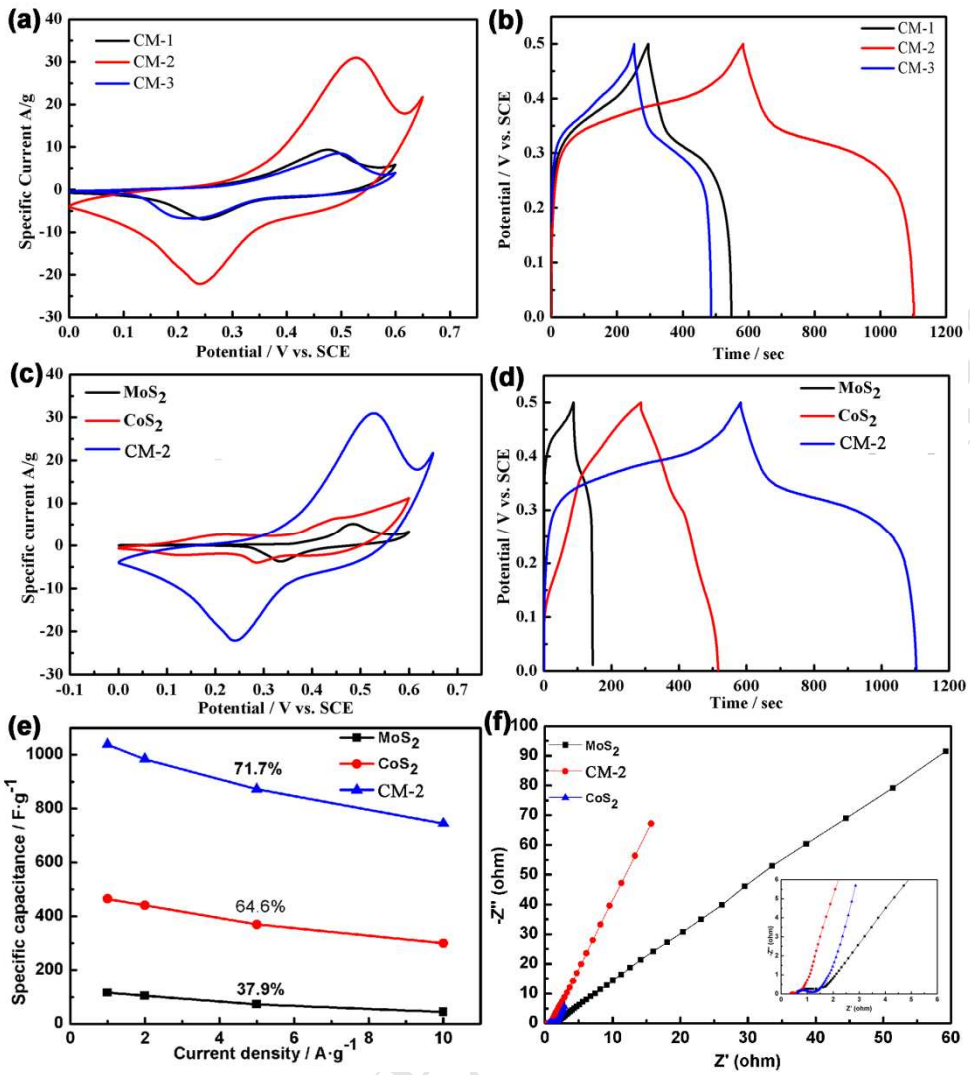
(a)
CM-1
CM-2
CM-3
Specific Current A/g
Potential / V vs. SCE
(b)
CM-1
CM-2
CM-3
Potential / V vs. SCE
Time / sec
(c)
MoS2
CoS2
CM-2
Specific current A/g
Potential / V vs. SCE
(d)
MoS2
CoS2
CM-2
Potential / V vs. SCE
Time / sec
(e)
MoS2
CoS2
CM-2
71.7%
64.6%
37.9%
Specific capacitance / F·g-1
Current density / A·g-1
(f)
MoS2
CM-2
CoS2
-Z'' (ohm)
Z' (ohm)

Figure 6

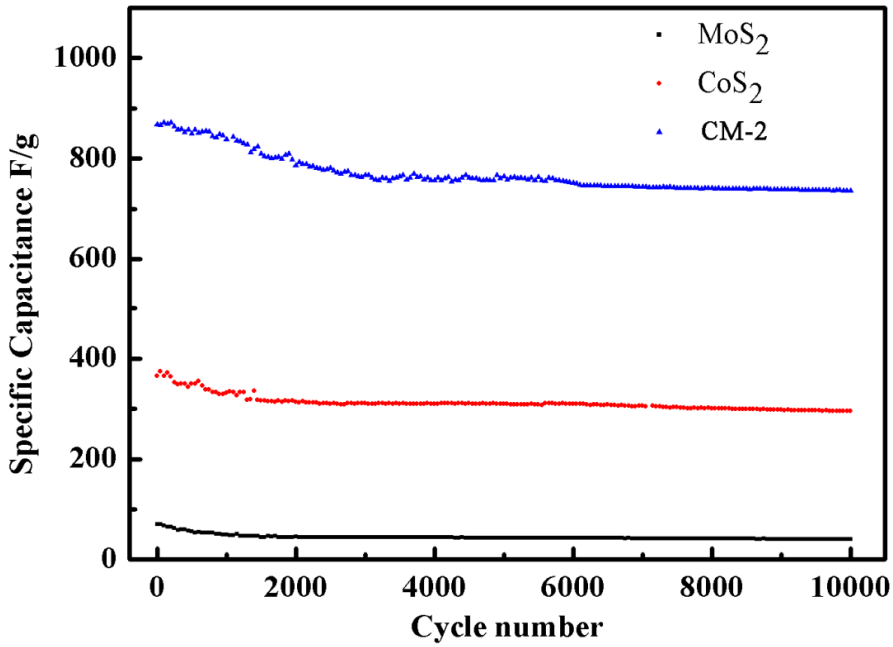

Figure 7

Highlights:

1. A MoS_2-coated CoS_2 composite has been prepared successfully via a one-step hydrothermal method.

2. The CoS_2@MoS_2 composite exhibits specific capacitance of 1038 F/g and rate capability of 71.7%.

3. The capacitance retention of CoS_2@MoS_2 composite equals 84.76% after 10000 cycles.